Universiteit Utrecht

IMAU
Institute for Marine and
Atmospheric research Utrecht

Faculty of Science

Verification of various Island Rules using simulations in application to the Indonesian Throughflow

BACHELOR THESIS

Franka Jesse
Physics and Astronomy

Supervisor:
Dr. A. von der Heydt
Institute for Marine and Atmospheric research Utrecht

June 2020

Abstract

The Indonesian throughflow is an important component of the upper cell of the global overturning circulation. It provides a pathway for warm, fresh waters from the Pacific Ocean to enter the Indian Ocean. Godfrey's Island Rule states that the transport through the Indonesian Archipelago can be estimated by integrating the surface wind stress around a path enclosing Australia. Study by Feng *et al.* (2017) suggests the throughflow is also influenced by deep Pacific upwelling and an amended Island Rule is proposed by them. In this thesis, we use simulations to verify both Godfrey's original Island Rule and the amended Island Rule. For our simulations, we use the four-degree model setup of Veros. Two model runs are conducted, each using different wind forcing. In both cases, we find that the amended Island Rule estimates the actual transport better than Godfrey's Island Rule does. Our results imply that deep Pacific upwelling does indeed contribute to the strength of the Indonesian throughflow. When studying the future climate under global warming, this should be taken into account to acquire a better estimate of the transport through the Indonesian Archipelago.

Contents

1 Introduction

The Indonesian Throughflow, hereafter referred to as the ITF, provides a low-latitude pathway for warm, fresh waters from the Pacific to enter the Indian Ocean [14, 26]. Therefore, the flow through the Indonesian passages has a great impact on the global climate. Study of Gordon (1996) [15] suggests that the return flow of the North Atlantic Deep Water is upwelled and warmed primarily within the ocean's warm thermocline and flows back via the ITF, which is therefore an important component of the upper cell of the global over-turning circulation. Furthermore, many authors suggest that the heat flux into the Indian Ocean may affect the Indian Ocean circulation regionally, and it may also affect both sea surface temperature and heat flux [13, 20]. Since the ITF affects the global ocean circulation, it is important to have a good understanding of the dynamical processes which drive the flow. For example, understanding these processes would give us more insights into the development of the ITF under global warming.

In Figure 1.1, the region's complex geography and the main currents contributing to the ITF are displayed. Due to the numerous islands and narrow passages it is difficult to determine the amount of water flowing through the Indonesian archipelago by observations. Because of these observational difficulties, analytical models are of great importance in analysing the ITF [22].
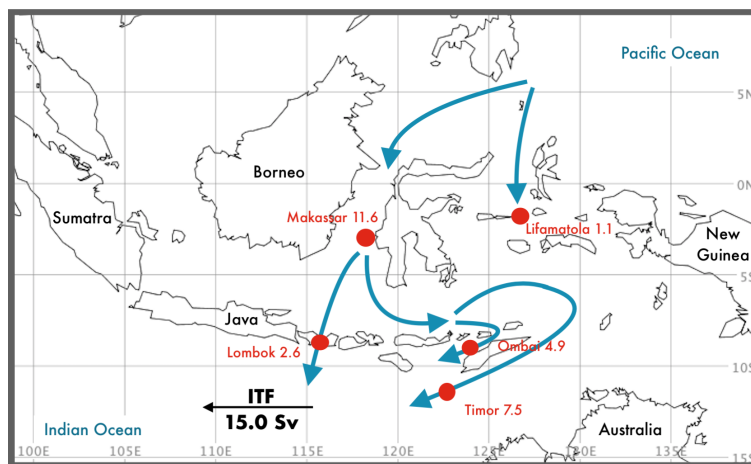

Figure 1.1: Schematic view of the transport of the main currents, represented by blue arrows, contributing to the Indonesian Throughflow. Numbers in red indicate the 3-year mean transport (from 2004 to 2006) in Sverdrups (Sv) through different passageways (values and directions from Sprintall *et al.* [26]).

In 1989, Godfrey derived an analytical relation to be able to estimate the flow around an island, nowadays known as the Island Rule [12]. Based on the Sverdrup balance, Godfrey's Island Rule relates large-scale ocean circulation to surface wind-stress curl forcing. His Island Rule is certainly applicable to the area we are looking at, as this is the region he designed it for. In this case, Australia is the island which the ITF flows around. Following the frictionless Island Rule, one can estimate the ITF transport by integrating wind stresses in the south Pacific and along the west coast of both Australia and of South America.

Over the years, the Island Rule has been widely used to assess the wind-driven ITF transport [5, 18]. In their study, Feng *et al.* (2017) [10] proposed an amendment on Godfrey's Island Rule, which led to a better estimation of the ITF. This amended Island Rule dictates that the strength of the ITF not only depends on wind-driven circulation, but also on deep Pacific upwelling, which results in an extra term to Godfrey's Island Rule.

In this thesis, we will investigate to what extent the outcome of both Godfrey's Island Rule and the amended Island Rule proposed by Feng *et al.* agree with the actual flow obtained from simulations. For the simulations we use the relatively new model "Veros", the Versatile Ocean Simulator, which is a general circulation

ocean model that was translated from Fortran to Python [16]. Both Island Rules will be tested in the global four-degree configuration, which incorporates fifteen vertical levels. Two model runs will be conducted, each with different wind forcing.

The remainder of this thesis is organised as follows. In Section 2, we provide some informational background on the ITF. Furthermore, we go through the derivation of Godfrey's Island Rule and discuss what led to the suggestion of the amended Island Rule. In Section 3, we will explain more about Veros and discuss our simulation setups. The results of the simulations are shown in Section 4. First, the results for Godfrey's Island Rule are shown, followed by the results for the amended Island Rule. Some points of discussion are explained in Section 5, after which a brief summary of our findings and the main conclusions are given in Section 6. Lastly, we will make a few suggestions for further research in Section 7.

2 Theoretical background

In this section, some background information on the ITF will be discussed. Moreover, we will take a look at the derivation of both Godfrey's Island Rule [12] and the amended Island Rule by Feng et al. [10].

2.1 Indonesian Throughflow and global ocean circulation

The ITF provides a low-latitude pathway for warm, fresh waters from the Pacific to the Indian Ocean. It is even considered to be the only major low-latitude connection in the global oceans [26]. Hence, the ITF plays a crucial role in the ocean circulation. The heat transport of the ITF cools the Pacific and warms the Indian Ocean. To give a better view of the position of the ITF in the global ocean circulation, Figure 2.1 is included. This figure shows the global conveyor belt, a system of ocean currents that transport water all around the globe. The deeper cold currents are driven by differences in water densities, which depend on both temperature and salinity. Whereas the warmer surface currents are mostly driven by wind.
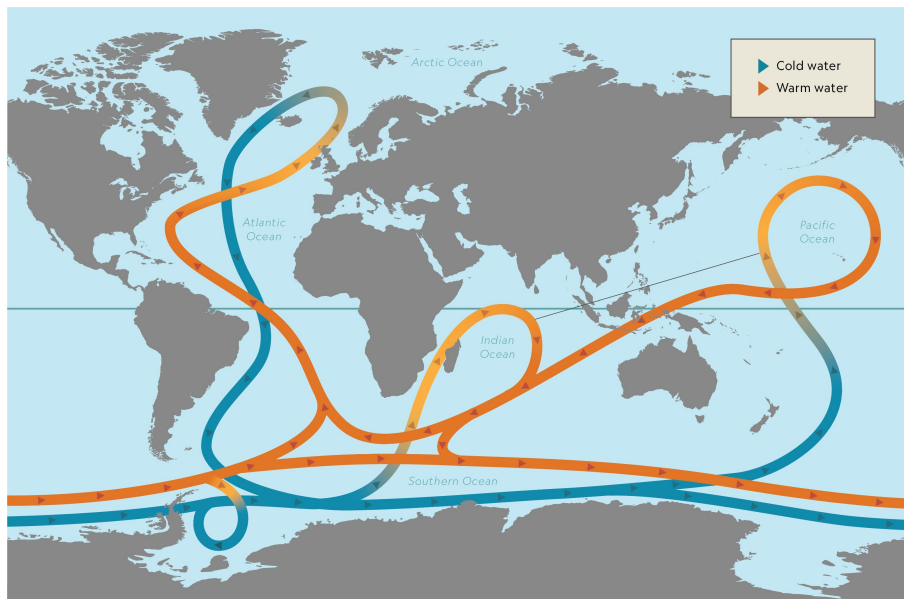

Figure 2.1: Schematic view of the global conveyor belt. Image from [1].

As mentioned in the introduction, the region's geography is very complex. In 1961, Wyrtki [29] provided the first estimate of the strength of the ITF in the top 200 meters of the ocean. His estimate was based on ship drifts, hydrographic observations, sea-level records and climatologic wind pattern. He estimated the strength of the flow in the top 200 meters to be about 1.7 Sv. Note that this is just a fraction of the values from more recent research as is displayed in Figure 1.1. Since the first attempt of Wyrtki, more research was done on determining the ITF transport. It is observed that the ITF experiences substantial interannual and decadal variations, influenced by the Pacific and Indian wind forcing. Study by Meyers (1996) [21] shows that there is a clear relationship between the ITF transport and the El Niño–Southern Oscillation (ENSO). The ITF transport is strengthened during La Niña and weakened during El Niño. Decadal variations of the ITF may be explained by the decadal climate models in the Pacific, such as the Pacific Decadal Oscillation or the Interdecadal Pacific Oscillation (IPO) [30]. Negative phase of the IPO is associated with stronger than normal trade winds, whereas positive phase is associated with weaker winds [9]. Direct measuring of the ITF transport and variability is challenging, but there have been studies that made an effort. The most extensive observations of the ITF have been done during the International Nusantara Stratification and Transport Program (INSTANT), where measurements were conducted in the major inflow and outflow passages. Results from Sprintall *et al.* [26] are displayed in Figure 1.1. Due to the complex geography, analytical ways to estimate the throughflow were proposed.

2.2 Godfrey's Island Rule

A first attempt to analytically estimate the ITF transport came from Godfrey in 1989. He proposed the Island Rule [12], relating the flow around a mid-ocean island to the surface wind-stress curl. This relation has often been used to estimate the strength of the ITF by integrating the surface wind stress following a path around Australia and up to the western coast of South America. We will now go through the theoretical derivation of Godfrey's Island Rule based on the publication of Pedlosky *et al.* in 1997 [23] and a publication of Wajsowicz in 1993 [28].

We start with a single layer of homogeneous fluid, which satisfies the horizontal momentum equation in the form:

$$\frac{\partial \boldsymbol{u}}{\partial t} + (\zeta + f)\hat{k} \times \boldsymbol{u} = -\boldsymbol{\nabla}\left(\frac{\rho}{p} + \frac{|\boldsymbol{u}|^2}{2}\right) + \boldsymbol{F} + \text{Diss}(\boldsymbol{u}), \tag{1}$$

where $\boldsymbol{u} = \boldsymbol{u}(u, v, t)$ is the flow velocity, ζ is the vertical component of the relative vorticity, f is the Coriolis parameter and $\hat{k}$ is a vertical unit vector. The first term of the right-hand side of Equation (1) is the gradient of the Bernoulli function. $\boldsymbol{F}$ represents the forcing, which is the wind stress per unit density divided by the fluid depth. Finally, the dissipation of horizontal momentum is represented by $\text{Diss}(\boldsymbol{u})$. It is important to point out that we assume that the motion is horizontally nondivergent and thus geostrophic.
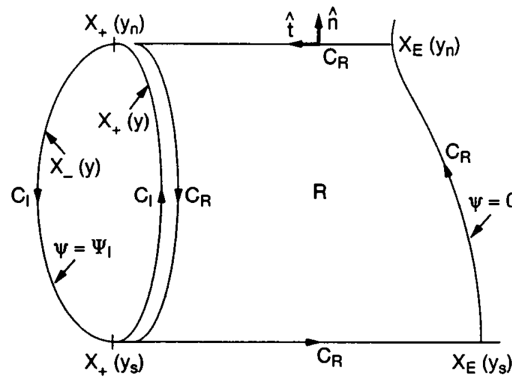

Figure 2.2: The contours C_I, around the island, and C_R, which enfolds the ocean basin east to the island. C_I and C_R coincide on the island's eastern boundary and run in opposite directions there. For clarity, C_R is shown slightly displaced from C_I. Figure from Pedlosky [23].

When an island exists in an ocean basin, it is interesting to look at the tangential component $\hat{t}$ of the momentum equation integrated around the island. This namely yields an equation for the circulation around the island. The velocity normal to the island is zero, which makes the tangential component of the total vortex force (the second term on the left-hand side of Equation (1)) vanish. The tangential component of the gradient of the Bernoulli function (the first term on the right-hand side of the equation) is an exact differential, which means it will vanish when integrated around a closed circuit. Thus integrating along the counterclockwise circuit, C_I (Figure 2.2), around the island, we obtain:

$$\frac{\partial}{\partial t}\oint_{C_I} \boldsymbol{u} \cdot \hat{t}\, ds = \oint_{C_I} \boldsymbol{F} \cdot \hat{t}\, ds + \oint_{C_I} \text{Diss}(\boldsymbol{u}) \cdot \hat{t}\, ds. \tag{2}$$

Following the suggestion of Godfrey (1989) [12], we also consider the contour C_R, running along the eastern boundary of the ocean basin between y_s and y_n and then westward along the latitude $y = y_n$ until it reaches the island. It follows the eastern boundary of the island and returns eastward along the latitude $y = y_s$. Just as before, we integrate in a counter-clockwise circuit. Again the Bernoulli function vanishes. However, the second term of Equation (1) only differs from zero on the open boundaries, so this term will stay. We obtain

$$\frac{\partial}{\partial t}\oint_{C_R} \boldsymbol{u} \cdot \hat{t}\, ds + \oint_{C_R} \zeta \boldsymbol{u} \cdot \hat{n}\, ds + \oint_{C_R} f\boldsymbol{u} \cdot \hat{n}\, ds = \oint_{C_R} \boldsymbol{F} \cdot \hat{t}\, ds + \oint_{C_R} \text{Diss}(\boldsymbol{u}) \cdot \hat{t}\, ds, \tag{3}$$

where $\hat{n}$ is the outward unit normal vector to the contour C_R. Note that the transport between the island and eastern boundary of the basin is independent of latitude for our barotropic incompressible fluid. This means we can rewrite the integral of the flux of planetary voriticity as following:

$$\oint_{C_R} f\boldsymbol{u} \cdot \hat{n}\, ds = f_n \int_{x-}^{x_E} v(x, y_n)dx - f_s \int_{x-}^{x_E} v(x, y_s)dx$$
$$= -(f_n - f_s)\psi_I, \tag{4}$$

where f_n is the Coriolis parameter on latitude $y = y_n$ and f_s the Coriolis parameter on latitude $y = y_s$. We have chosen the stream function to be constant, $\psi = \psi_I$, around the island and zero, $\psi = 0$, on the eastern boundary of the basin.
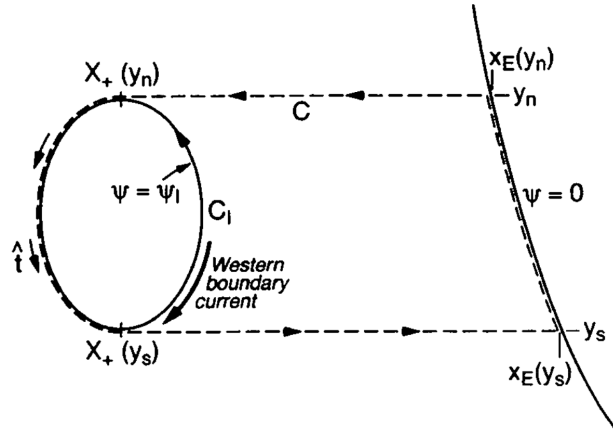

Figure 2.3: Contour C, which is the sum of C_I and C_R from Figure 2.2. Contour C runs along the latitudes y_n and y_s, follows the western boundary of the island and then closes along the eastern boundary of the basin. Figure from Pedlosky [23].

By taking the sum of the integrals for contour C_I (Equation (2)) and contour C_R (Equation (3)), we obtain an expression for the flow around the island ψ_I. The portions of the integrals along the eastern boundary of the island will cancel each other since they run in opposite directions. What we will be left with is contour C, displayed in Figure 2.3. Adding the integrals and using Equation (4), we obtain

$$\frac{\partial}{\partial t} \oint_C \boldsymbol{u} \cdot \hat{t}\, ds + \oint_C \zeta \boldsymbol{u} \cdot \hat{n}\, ds - (f_n - f_s)\psi_I = \oint_C \boldsymbol{F} \cdot \hat{t}\, ds + \oint_C \text{Diss}(\boldsymbol{u}) \cdot \hat{t}\, ds. \tag{5}$$

Since we are interested in the flow around the island ψ_I, we rewrite this as:

$$(f_n - f_s)\psi_I = \frac{\partial}{\partial t} \oint_C \boldsymbol{u} \cdot \hat{t}\, ds + \oint_{C_R} \zeta \boldsymbol{u} \cdot \hat{n}\, ds - \oint_C \boldsymbol{F} \cdot \hat{t}\, ds - \oint_C \text{Diss}(\boldsymbol{u}) \cdot \hat{t}\, ds. \tag{6}$$

When the circulation has reached a steady state, the first term on the right-hand side of Equation (6) vanishes due to the partial time derivative. When nonlinearity is negligible, which is plausible since we avoid the Western boundary currents, the second term also vanishes. Assuming dissipation can be ignored, the last term is crossed out as well. Using Sverdrup balance, which relates vertically-integrated meridional flow to the curl of the wind stress [19], Equation (6) then reduces to

$$\psi_I = -\frac{1}{f_n - f_s} \oint_C \frac{\tau^t}{\rho_0}\, ds, \tag{7}$$

using $\tau^t = \boldsymbol{\tau} \cdot \hat{t}$ for the along route wind stress in Newtons per square meter and ρ_0 the mean water density in kilograms per cubic meter. Since the flow around the island is in a counterclockwise direction, the stream

function will give a negative value [11]. Therefore, the absolute value of Equation (7) is used to represent the actual transport:

$$T_{ITF} = \frac{1}{f_n - f_s} \oint_C \frac{\tau^t}{\rho_0} \, ds. \tag{8}$$

We find that (under the condition that the flow has reached a steady state, nonlinearity is negligible and dissipation can be ignored) the flow around the island can be calculated from the annual mean wind stress following contour C. We will be referring to Equation (8) as Godfrey's Island Rule from now on.

2.3   Amended Island Rule

We mentioned the interannual and decadal, mostly wind driven, variations of the ITF in Section 2.1. However, there have been model projections of a declining trend of the ITF which can not be explained by the wind-driven circulation [4]. Study by Vecchi *et al.* [27] suggests a weakening trend of Pacific winds of about 3,5%. Sen *et al.* [24] states that the projected ITF decrease can not be explained by this change in regional winds alone. They suggest that the declining trend in the future climate can not be determined by Godfrey's Island Rule only, but is associated with a weakening trend of deep water formation in the Southern Ocean and a slowdown of upwelling in the deep Pacific Ocean.

In a paper by Feng *et al.* (2017) [10] this relation was formalised to an amended Island Rule. An assumption that is made in Godfrey's Island Rule is that the ocean is inert below the depth of integration that represents the depth of the wind-driven flow. Feng *et al.* propose to relax this assumption and recognize that the deep ocean does communicate with the upper ocean through basin-wide upwelling. To include Pacific upwelling they proposed the amended Island Rule:

$$T_{ITF} = \frac{1}{f_n - f_s} \oint_C \frac{\tau^t}{\rho_0} ds + \iint_{Pacific} w_Z \, dl \,, \tag{9}$$

with w_Z the vertical velocity at a certain depth z. In the paper by Feng *et al.* (2017) they used an eddy-rich ocean model to verify the amended Island Rule. They chose to integrate the vertical velocity at a depth of 1500 meters, since this best best defines the boundary between Antarctic Intermediate Water (AAIW) and deep Pacific Deep Water (PDW) as is shown in Figure 2.4. They showed that the weakening of deep upwelling in the Pacific is the main contributor to the weakening trend of the ITF transport.
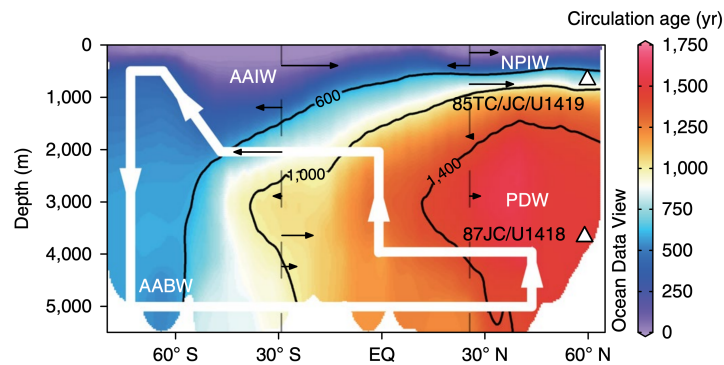

Figure 2.4: A meridional (138W) section of circulation age in the Pacific to indicate the locations of Pacific Deep Water (PDW) and Antarctic Intermidate Water (AAIW). Figure from Du *et al.* [7].

3 Method

In order to verify both Island Rules we use numerical simulations. In this section we will discuss the ocean model we used and the setup for our simulations.

3.1 Description of Veros

The simulations are performed using the Versatile Ocean Simulation in pure Python (Veros), which is an uncoupled ocean model. At its numerical core, Veros is a direct translation of pyOM2, a primitive equation finite-difference ocean model with a special emphasis on energetic consistency [16]. Where pyOM2 consists of a backend written in Fortran 90, Veros runs everything in pure Python. Veros is designed to be approachable, powerful, and easy to adapt. Anyone with some experience in Python should be able to set up, control and post-process Veros. It aims to support a wide range of problem sizes and architectures, and for this, Python is a great fit.
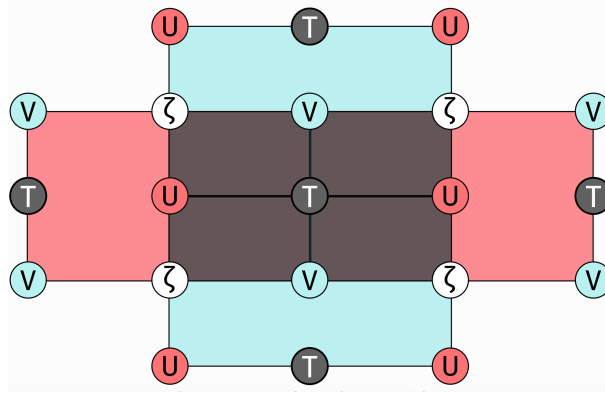

Figure 3.1: The structure of the Arakawa C-grid used in Veros. Image from [2].

The numerical solutions in Veros are calculated using finite differences on an Arakawa C-grid, as is shown in Figure 3.1. This grid is staggered in every dimension. Tracers (like salinity and temperature) are calculated at different positions than zonal, meridional and vertical fluxes (like velocities u, v and w). What we are interested in, is the two-dimensional barotropic stream function Ψ of the vertically integrated flow. In Veros, Ψ is calculated in every iteration of the solver to account for effects of the surface pressure. It can be obtained by solving a two-dimensional Poisson equation of the form:

$$\Delta \Psi = \int_0^{h(x,y)} \zeta(x,y,z)\,dz, \tag{10}$$

with coordinates x, y, z, total water depth h, vorticity ζ and Laplacian Δ. In Veros the discrete version of this Laplacian is solved as follows [8]:

$$\Delta \Psi_{i,j} = \frac{\Psi_{i+1,j} - \Psi_{i,j}}{h_{i+1,j}^v \cos^2\left(y_j^u\right) \Delta x_{i+1}^t \Delta x_i^u} - \frac{\Psi_{i,j} - \Psi_{i-1,j}}{h_{i,j}^v \cos^2\left(y_j^u\right) \Delta x_i^t \Delta x_i^u}$$
$$+ \frac{\cos\left(y_{j+1}^t\right)}{\cos\left(y_j^u\right)} \frac{\Psi_{i,j+1} - \Psi_{i,j}}{h_{i,j+1}^u \Delta y_{j+1}^t \Delta y_j^u} + \frac{\cos\left(y_j^t\right)}{\cos\left(y_j^u\right)} \frac{\Psi_{i,j} - \Psi_{i,j-1}}{h_{i,j}^u \Delta y_j^t \Delta y_j^u}, \tag{11}$$

with the discrete stream function $\Psi_{i,j}$ at the ζ cell with indices (i,j). Latitude x and longitude y are each defined at T cells $(x_{i,j}^t, y_{i,j}^t)$ and U/V cells $(x_{i,j}^u, y_{i,j}^u)$. Furthermore grid spacings of T cells are given by $(\Delta x_{i,j}^t, \Delta y_{i,j}^t)$ and grid spacings of U/V cells are given by $(\Delta x_{i,j}^u, \Delta y_{i,j}^u)$ in each horizontal direction.

For a more specific overview on Veros, the reader is referred to the documentation of pyOM2 [8].

3.2 Simulation setup

As mentioned above, Veros supports a wide range of model configurations. In this thesis, we chose to work with the four-degree model because this can be run on a personal laptop without any difficulties. As the name suggests, this configuration uses a $4.0° \times 4.0°$ horizontal grid. Additionally, the model incorporates 15 vertical levels. The model extends latitudinally from 80S to 80N. This leads to $90 \times 40 \times 15$ grid elements in this configuration.

(a) Simple global bathymetry

(b) Simple regional bathymetry
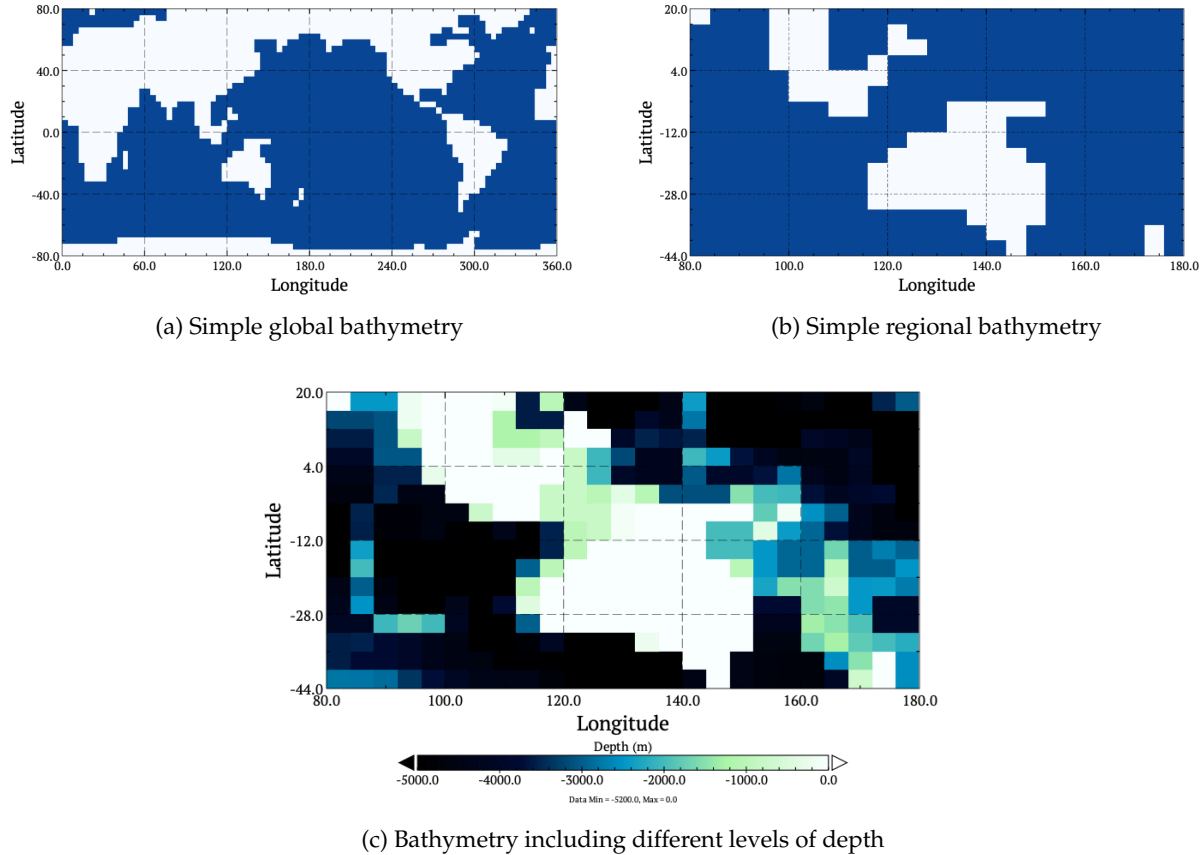

(c) Bathymetry including different levels of depth

Figure 3.2: The bathymetry data used for our simulations. In (a) and (b) the white grid cells represent land and blue cells represent water. In (c) we also a view of different depths is given.

NetCDF4-files containing forcing and heat flux data are used as input data. The heat flux data and forcing data are based on data from the European Centre for Medium-Range Weather Forecasts (ECMWF), also used in the basic model setups for pyOM2 [3]. The forcing data includes the bathymetry, which had a closed ITF in the original input data. To open the ITF, we modified the model by replacing a few land cells with water. Figure 3.2 shows the bathymetry we used. Notice that there is only one passage for the ITF, as opposed to reality, where the flow is distributed through multiple passages as shown in Figure 1.1.

Two different simulations were run, each using different wind forcing. For the first simulation, which we will call WIND1, we used wind forcing data based on the ECMWF. For the second simulation, WIND2, we used doubled wind forcing to study how the ITF would develop with increased wind and to see if both Island Rules would still give a good estimate. WIND2 is restarted from the restart file of WIND1 after 1000 years, using a new forcing with the before mentioned doubled wind. We restart the system from the existing integration because starting a new simulation with the doubled wind would perturb the system too much. The wind forcing files have 12 time steps, which represent different months. Wind forcing data for January and July for both WIND1 and WIND2 is shown in Figure 3.3 on the next page. Note the strong westerlies
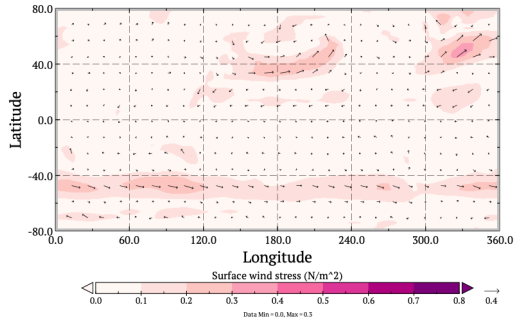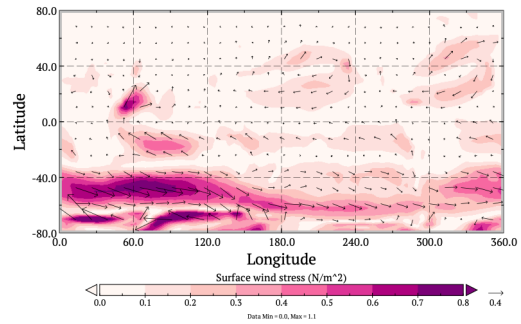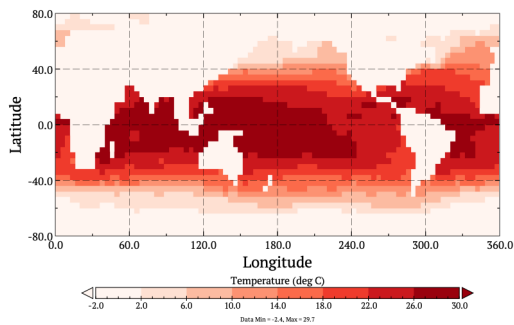
(a) Wind forcing in January for WIND1
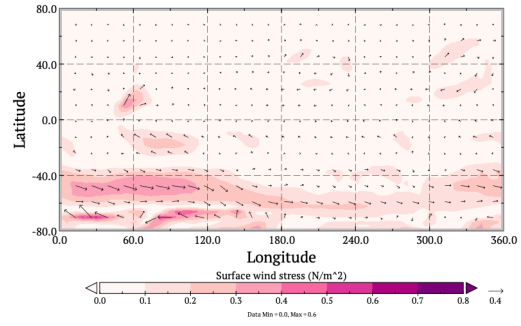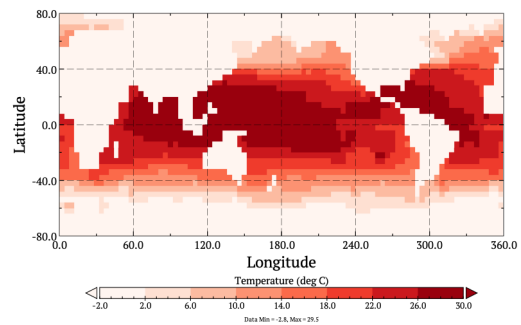
(b) Wind forcing in July for WIND1
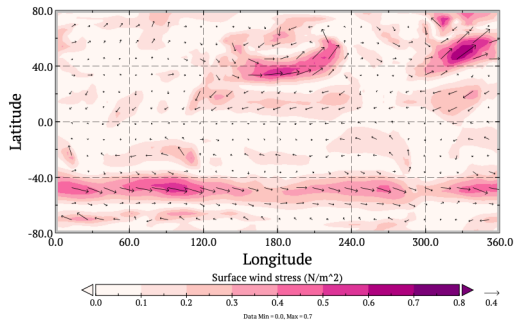
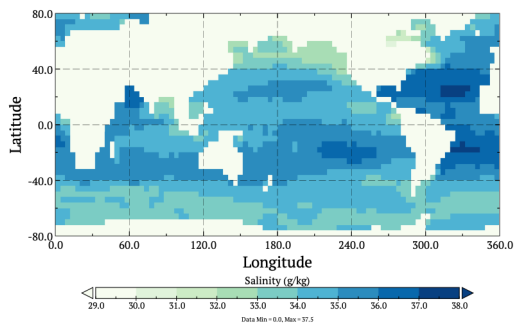(c) Wind forcing in January for WIND2

(d) Wind forcing in July for WIND2

(e) Sea surface temperature forcing (SST) in January

(f) Sea surface temperature forcing (SST) in July

(g) Sea surface salinity forcing (SSS) in January
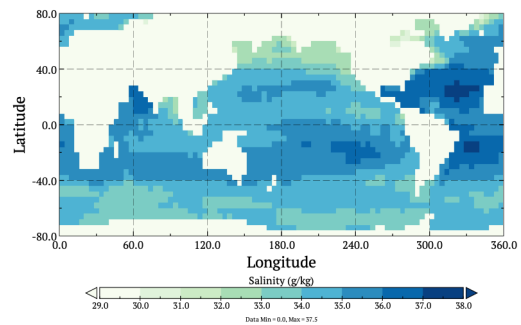
(h) Sea surface salinity forcing (SSS) in July

Figure 3.3: Prescribed wind forcing for WIND1 in January (a) and July (b). Prescribed wind forcing for WIND2 in January (c) and July (d), where the wind is doubled relative to WIND1. Sea surface temperature forcing (SST) in January (e) and July (f) and the sea surface salinity forcing (SSS) in January (g) and July (h). Forcing data is based on data from the ECMWF, also used in the pyOM2 setup [3].

between latitude 30S and 60S. They have a great impact on the circulation in the Southern Ocean [17]. Apart from the wind, the forcing data is the same for both simulations. The forcing for sea surface temperature and sea surface salinity also consist of 12 time steps. The data for January and July is also displayed in Figure 3.3. A seasonal shift is seen in the temperature forcing, where we see an increase of temperature in the Northern Hemisphere in July relative to January. Consistent forcing is used for every simulation year.

The output is written to several NetCDF4-files, which we can easily analyse in both Python and Panoply, a software tool developed by NASA that is able to plot geo-referenced and other arrays from NetCDF4-files. The output data is written to four different files: averages, energy, snapshot and overturning. The data output we analyse to compute the Island Rule and analyse the actual throughflow is in the averages file. This file contains annual averages of surface wind stress τ^x and τ^y, velocities u, v and w, stream function Ψ, temperature and salinity. Furthermore, we will be using the overturning file to analyse the meridional overturning circulation.

To compute the integral of the Island Rule, we need the surface wind stress data τ^x and τ^y calculated at the U and V cell respectively. For the amended Island Rule, we need the vertical velocity data w, which is calculated at the T cell. To obtain the actual flow, we analyse Ψ, which is calculated at the ζ cell (Figure 3.1), as explained in Section 3.1.

By taking the difference of the Ψ value for two grid cells, the transport between these grid cells is computed. In our case, the model was not writing output to boundary cells and therefore the stream function did not look good at first, namely displaying varying values around coastlines. By comparing our simulation out-come to new simulations where this problem was fixed, we found that the grid cell at $[x = 128, y = -8]$ (denoted by a yellow cross in Figure 4.2) best represents the transport of the ITF with a small error of about +0.2 Sv, compared to the new simulations. More on this is found in Appendix A.

To compute the estimate from Godfrey's Island Rule, we integrate the sea surface wind stress along contour ABCD, shown in Figure 3.4. This will be our contour C, which was discussed in Section 2.2. We use the values listed in Table 3.1 for the Coriolis parameters and the mean water density.
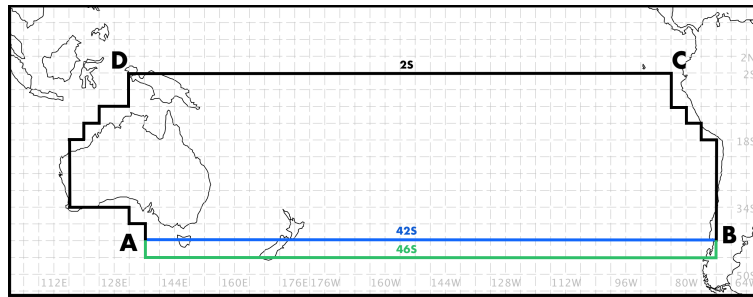
Figure 3.4: Path ABCD delineates the integration route for the wind stress in the Island Rule calculation. We will compare two routes, one where AB is at 42S (blue) and one where AB is at 46S (green).

Parameter	Value
f_n	-0.051×10^{-4} s^{-1}
f_s at 42S	-0.973×10^{-4} s^{-1}
f_s at 46S	-1.046×10^{-4} s^{-1}
ρ_0	1000 kg/m^3

Table 3.1: Values for different Coriolis parameters and water density, used to compute the transport in both Island Rules.

To compute the amended Island Rule, we need to add the Pacific upwelling north of segment AB to God-frey's Island Rule. In the study of Feng *et al.* (2017) a depth of integration of 1500 meters was chosen, as this level identifies the level between deep ocean circulation and the upper ocean circulation [10]. Since we are working with a lower resolution model, we will compute the integration for 1080 meters, 1420 meters and 1810 meters and compare these outcomes.

Both simulations were run for 1800 years to give the system time to get into equilibrium. We need the flow to be in equilibrium since the Island Rule assumes the flow to be in a steady state. We had expected the flow to reach equilibrium after about 1000 years.

4 Results

The results are discussed in three parts. First, the actual flow, computed with stream function Ψ, is compared to the predicted flow resulting from Godfrey's Island Rule. Secondly, the actual flow is compared to the amended Island Rule. Lastly, the percentage of deviation of both Island Rules for both simulations is presented.

4.1 Godfrey's Island Rule

As explained in Section 3.2, two simulation runs, each lasting 1800 years, were executed. In this section, the estimated transport calculated with Godfrey's Island Rule is compared to the actual flow, which is computed using the stream function Ψ.

First, we discuss the values computed with Godfrey's Island Rule. Figure 4.1 shows the annual averaged surface wind stress for both simulations. Note that for WIND2 in Figure 4.1b the values are simply doubled compared to the values of WIND1 in Figure 4.1a. We see the strong westerlies between 30S and 60S, which drive the circulation in the Southern Ocean [17].

Integrating the wind stress around path ABCD (Figure 3.4) for both WIND1 and WIND2, we obtain the results displayed in Table 4.1. Earlier research by Sprintall *et al.* found an average transport of $15\,\mathrm{Sv}$ [26]. We see that the estimate for WIND1 does not deviate more than $3\,\mathrm{Sv}$ from this value when calculated using Path 42.

	WIND1 (Sv)	WIND2 (Sv)
Path 42S	17,860207	35,720413
Path 46S	21,005662	42,011324

Table 4.1: Results for the ITF transport in Sverdrups (Sv) using Godfrey's Island Rule at Path 42S and Path 46S for both simulations. The first column lists the different integral routes. In the second and third column, the estimated strength of the transport for WIND1 and WIND2 are listed respectively.

In Table 4.2, the contribution of different segments to the ITF transport are listed for Path 42S and Path 46S. We see that segment AB contributes most to the ITF transport for both integral routes. Looking at Figure 4.1 this makes sense since the wind stress along segment AB has a relative large zonal component due to the strong westerlies. Segment BC contributes about 15% - 20%, this is due to the southerly wind along the coast of South-America. The contribution of segment CD is comparable to the contribution of BC. Segment DA contributes least with about 4-5%. Note that for Path 46S the contribution of segment AB is relatively larger than for Path 42S. This can be explained by the fact that the westerly winds are significantly stronger at this latitude (Figure 4.1).

segments	Path 42S	Path 46S
AB	55,57%	63,81%
BC	19,77%	14,81%
CD	20,68%	16,30%
DA	3,97%	5,10%

Table 4.2: The contribution of different segments to the ITF transport. The first column lists the different segments from Figure 3.4. In the second and third column, the results for Path 42S and Path 46S are listed respectively. The fractions following the segments give the relative contribution to the transport.
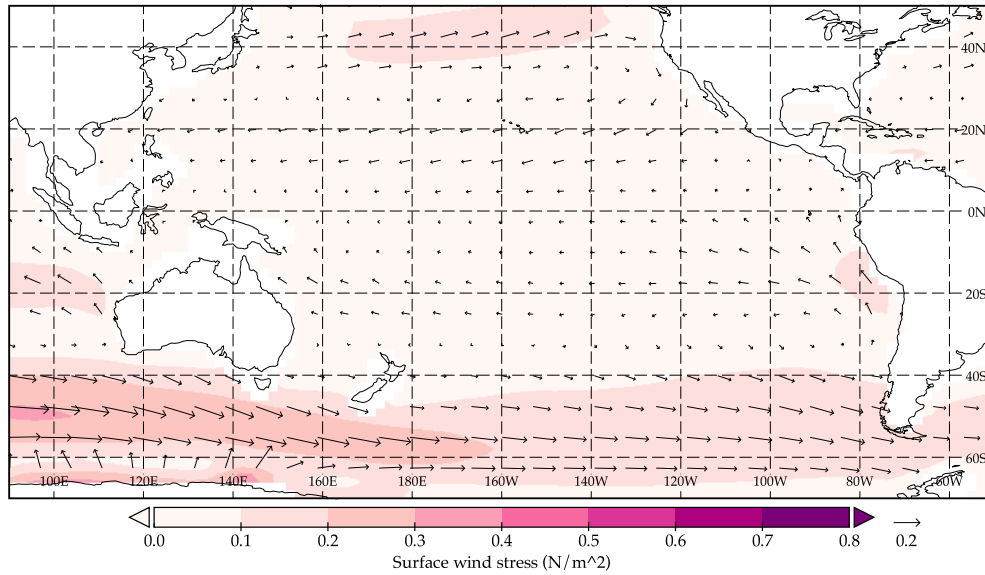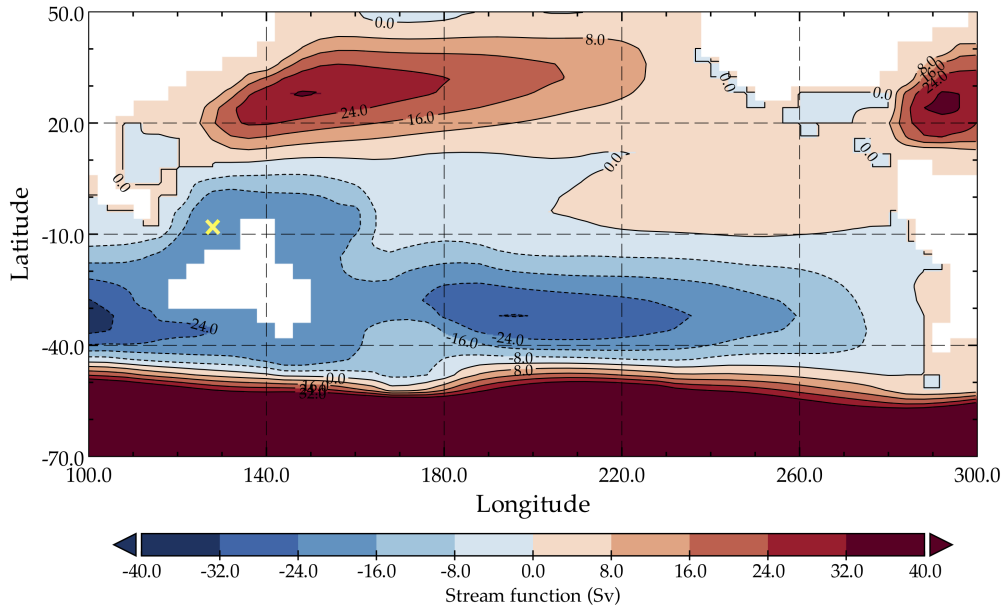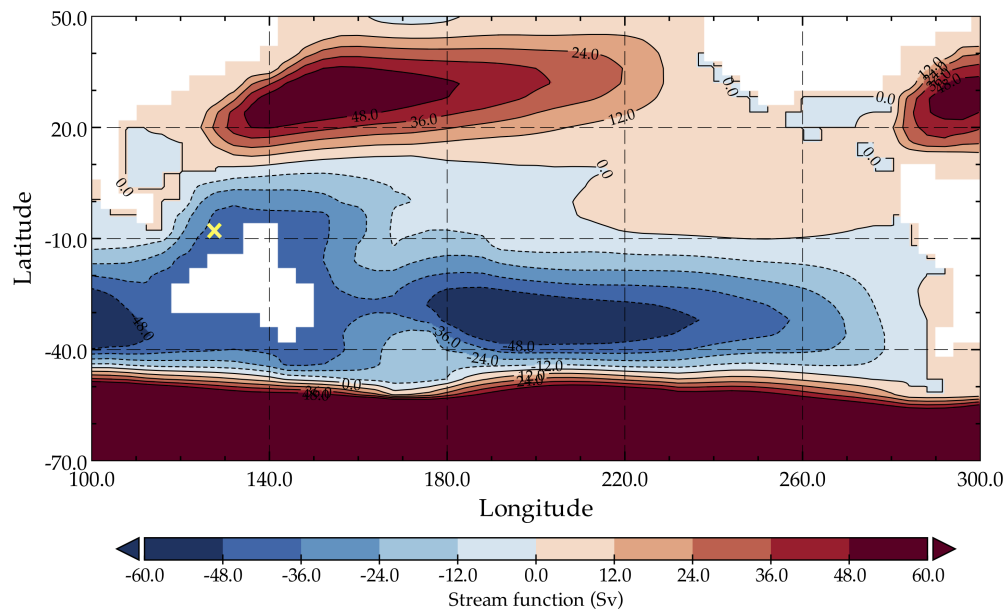
(a) Simulation output of WIND1
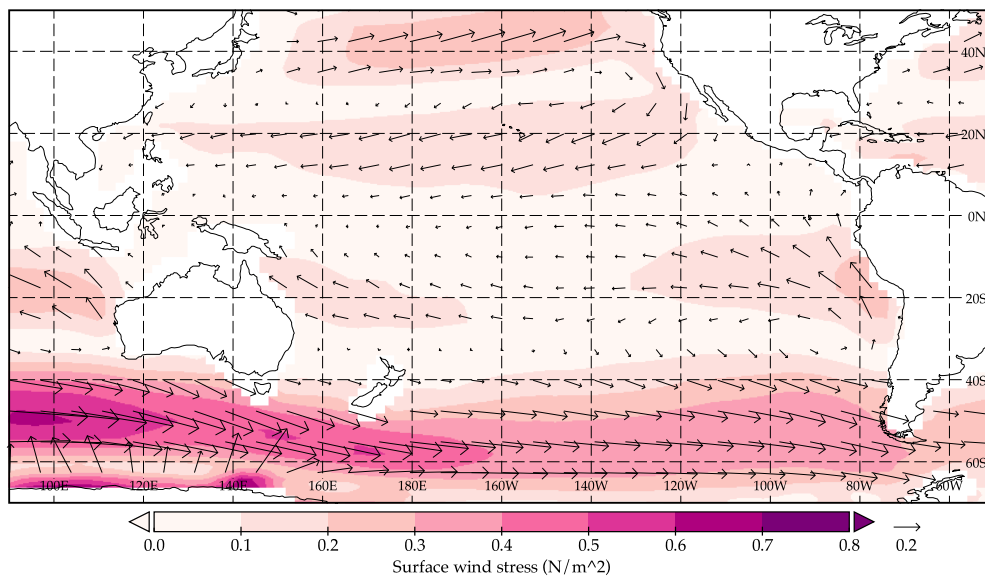
(b) Simulation output of WIND2

Figure 4.1: Annual averaged surface wind stress for simulation WIND1 (a), using normal wind forcing and for simulation WIND2 (b), using doubled wind forcing.

To obtain the actual flow, we analyse the stream function Ψ. A contour plot of Ψ is shown for both WIND1 and WIND2 at 1400 years in Figure 4.2. Note that the stream function is negative in the region of the ITF, indicating a counterclockwise flow. This agrees with observations where western tropical Pacific water flows to the southeastern tropical Indian Ocean [25].

(a) Simulation output of WIND1

(b) Simulation output of WIND2

Figure 4.2: Contour plot of the annual averaged stream function Ψ in Sverdrups at 1800 years for simulation WIND1 (a), using normal wind forcing and for simulation WIND2 (b), using doubled wind forcing. Note that the scale in (a) differs from the scale in (b). The yellow cross in both figures indicate the coordinate $[x = 128, y = -8]$, the grid cell of which we take the Ψ-value to calculate the actual flow.

(a) Global MOC for WIND1 after 1800 years

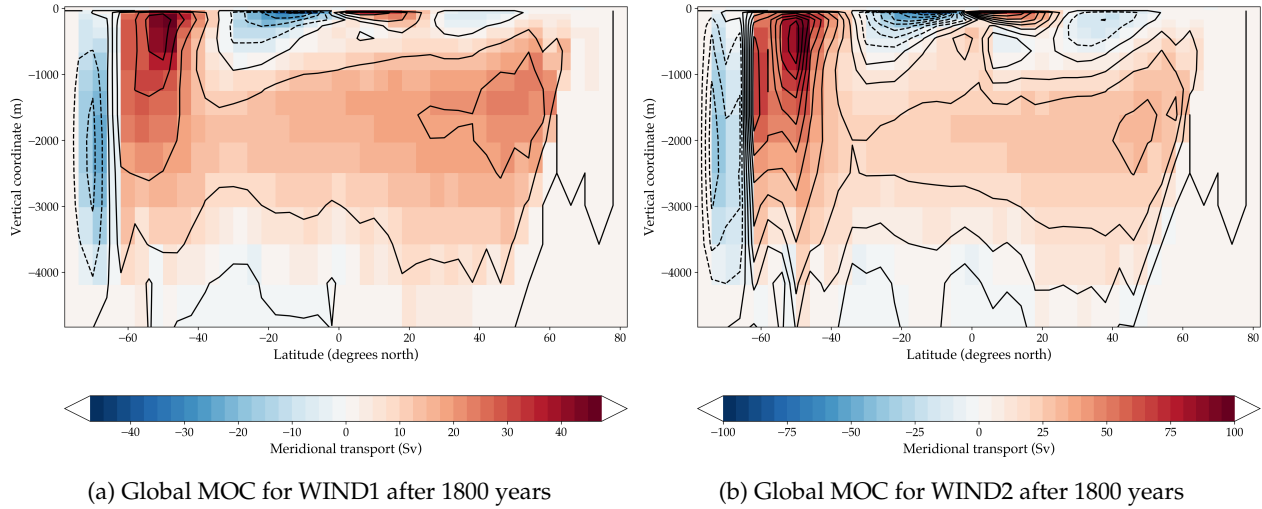(b) Global MOC for WIND2 after 1800 years

Figure 4.3: Contour plot of the Global Meridional Overturning Circulation (MOC) after 1800 years for WIND1 (a) and WIND2 (b) in Sverdrups (Sv). Contour lines are displayed for every $10\,\mathrm{Sv}$. Dotted contours indicate negative values. Note that the scale in (a) differs from the scale in (b).

(a) MOC strength at 20N for WIND1
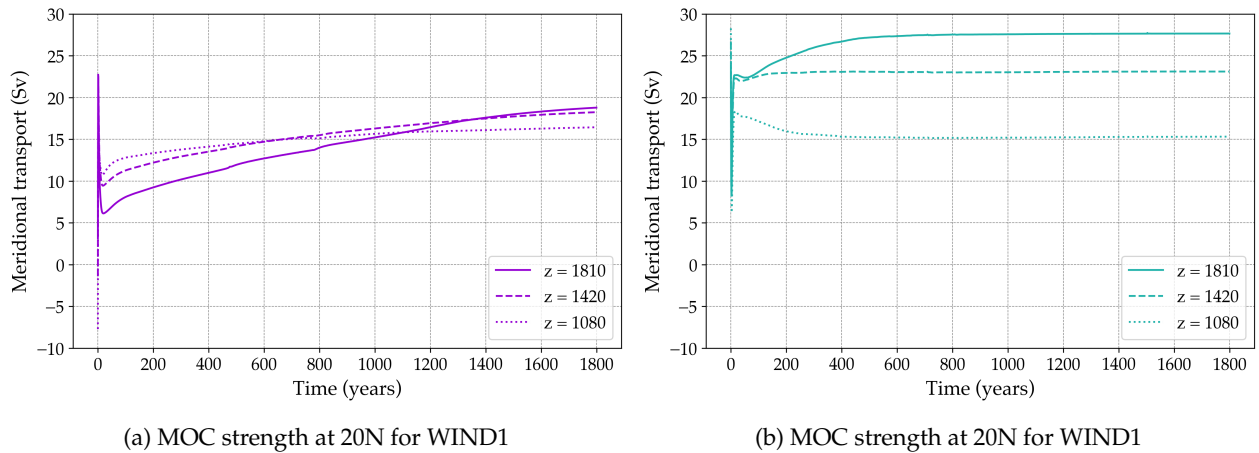
(b) MOC strength at 20N for WIND1

Figure 4.4: Time series of the meridional transport in Sverdrups (Sv) at latitude 20N for three different depths $[z = -1810\,\mathrm{m}, z = -1420\,\mathrm{m}, z = -1080\,\mathrm{m}]$ for both WIND1 (a) and WIND2 (b).

Additionally, we take a look at the Meridional Overturning Circulation (MOC). The global MOC after 1800 years for both WIND1 and WIND2 is shown in Figure 4.3a and Figure 4.3b respectively. Note that the scales differ for both Figures. We see that the MOC is stronger with doubled wind. In Figure 4.4 we see the meridional transport for latitude 20N for different depths. In Figure 4.4a, we see the results for WIND1. We can see an increasing trend in the meridional transport for all three depths, indicating that the deep ocean has not reached equilibrium yet. In Figure 4.4b, we see the results for WIND2. We see that in this case, the MOC has reached a steady state after 800 years for all three depths. We will now compare the actual flow to the Island Rule for both simulations separately.

4.1.1   WIND1: Normal wind

First, we consider the simulation with normal wind forcing, WIND1. In Figure 4.5a, we see the annual mean transport in Sverdrups plotted against time for a simulation run of 1800 years. The dashed blue and green lines represent the strength calculated by Godfrey's Island Rule for Path 42S and Path 46S respectively. The exact values are found in Table 4.1. The solid black line represents the actual flow computed with stream function Ψ, as is explained in Section 3.2.

Looking at the actual flow, we see that the time to spin up the ITF is approximately 400 years. From then on it seems to be stable with a strength of about $21, 25$ Sv, but after 1000 years the flow seems to strengthen again to a strength of 23 Sv and even higher. The flow does not reach a steady state in these 1800 years. This could be explained by the fact that the deep ocean is not in equilibrium yet as is shown in Figure 4.4a. The meridional transport in these figures is increasing and so does the transport of the ITF. The flow seems to be larger than it is in reality, where it is estimated to be about 15 Sv [26]. This could be explained by the fact that the flow in our simulation is not blocked by smaller islands and does not have to split into smaller streams. Additionally, the total ITF in our model is wider than in reality.
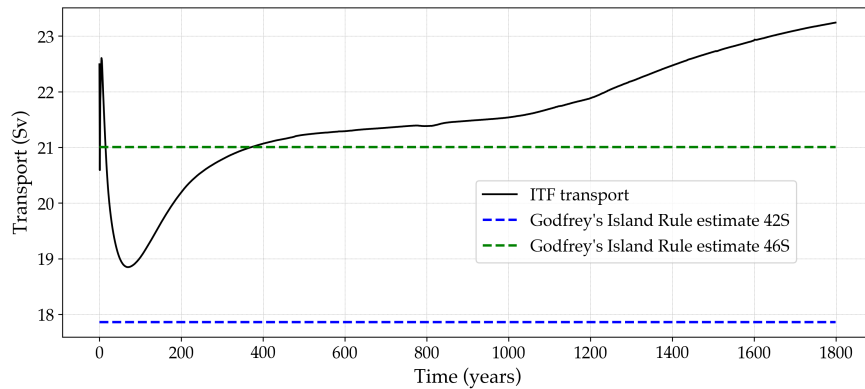
(a) Results for simulation WIND1
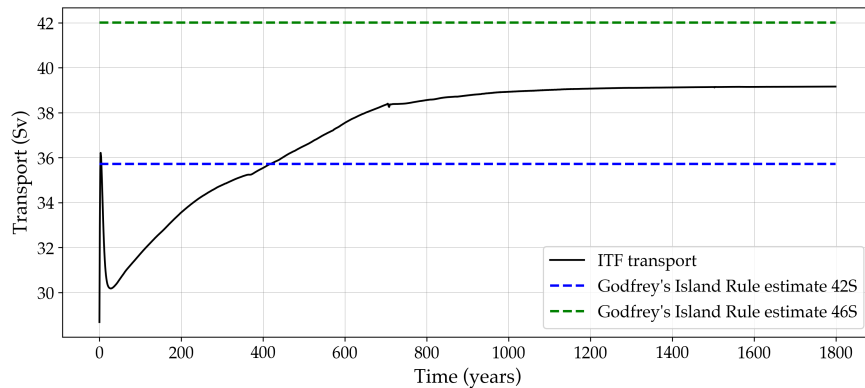
(b) Results for simulation WIND2

Figure 4.5: Time series of the ITF transport for a simulation with normal wind forcing (a) and with doubled wind forcing (b). In black the ITF transport computed with stream function Ψ is displayed. In blue and green the estimated transport by Godfrey's Island Rule for Path 42S and Path 46S respectively is shown.

The Island Rule predicts a constant strength of the flow because of the constant annual mean wind stress.

We see that the Island Rule for both paths estimates a strength of the same order of magnitude as the actual transport. The estimation, using Path 42S, is 1 to 5 Sv weaker than the actual flow. Considering the flow after 400 years, we see that the Island Rule at Path 46S estimates the flow quite well from year 400 until year 1000. During these years the Island Rule at Path 46S deviates 0 to $0,5$ Sv from the actual flow, however after 1800 years it deviates more than 2 Sv.

4.1.2 WIND2: Doubled wind

The results for the second simulation are shown in Figure 4.5b. We see that the strength of the ITF with doubled wind forcing is significantly larger than for WIND1. From this, we can conclude that the wind does have a significant influence on the transport through the Indonesian seas. After 1000 years, the flow seems to have reached a steady state. This is also the moment at which the deep ocean has reached equilibrium (Figure 4.4b). Both estimates from Godfrey's Island Rule deviate about 3 Sv from the actual flow. We observe that the Island Rule at Path 42S estimates the flow to be weaker than it actually is, whereas the Island Rule at Path 46S estimates the flow to be stronger.

4.2 Amended Island Rule

In this section, we will analyse the results of the amended Island Rule. The amended Island Rule (Equation (9)) includes the contribution from deep ocean vertical transport, in other words, the Pacific upwelling. The computed upwelling is displayed in Figure 4.6. We chose to look at three different vertical levels, as we do not know the precise depth which best represents the thermocline. Feng *et al.* (2017) chose to integrate the vertical speed at a depth of 1500 meters. This led to choosing our depths of 1080, 1420 and 1810 meters. The solid lines represent the amount of Pacific upwelling in simulation WIND1, the dashed lines represent the Pacific upwelling in simulation WIND2. The upwelling is plotted separately for Path 42S and Path 46S. The reason for this is that the upwelling has to be calculated north of segment AB, which is located at different latitudes.

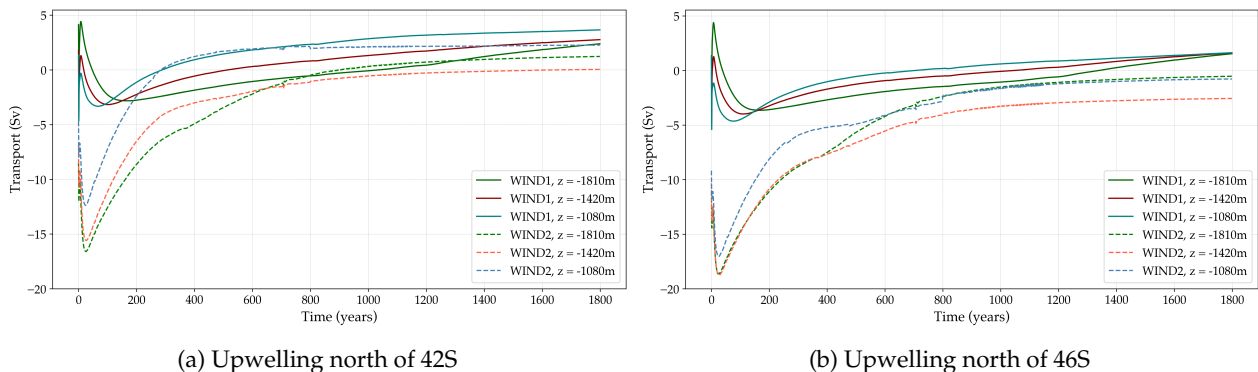(a) Upwelling north of 42S   (b) Upwelling north of 46S

Figure 4.6: Time series of the integrated vertical velocity at different depth levels in the Pacific Ocean north of 42S (a) and north of 46S (b). Solid lines represent the results for WIND1, dashed lines represent the results for WIND2.

We see that the annual mean vertical transport is negative in the first few hundred years. The circulation in the deep ocean needs much more time to spin up than the surface does. For WIND2 the upwelling seems to have reached a steady value, whereas for WIND1 the upwelling seems to increase in time. This difference between the two simulations was also observed in Figures 4.4a and 4.4b. Note that the upwelling north of Path 42S is stronger than the upwelling north of Path 46S. The results for the upwelling are added to Godfrey's Island Rule to obtain the results for the amended Island Rule. These results are discussed separately for both simulations.
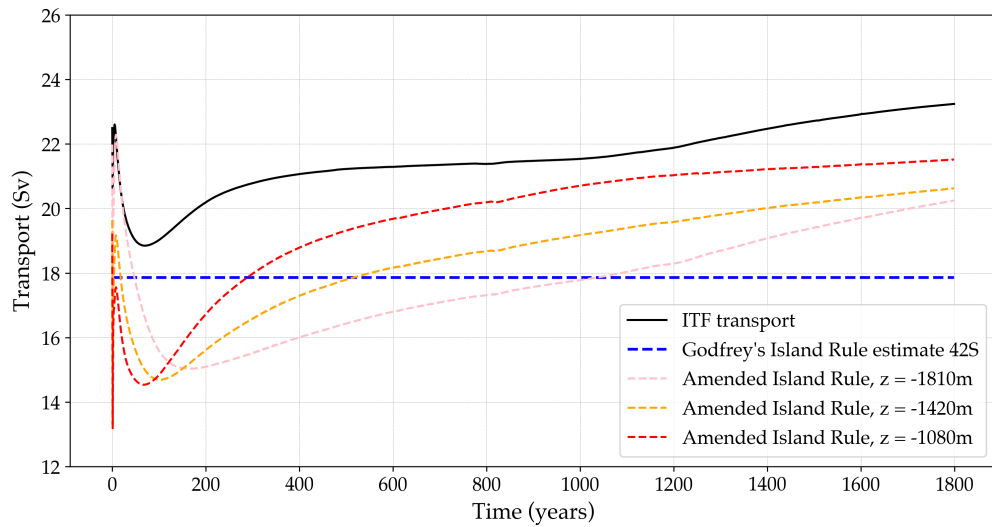
(a) Results for Path 42S
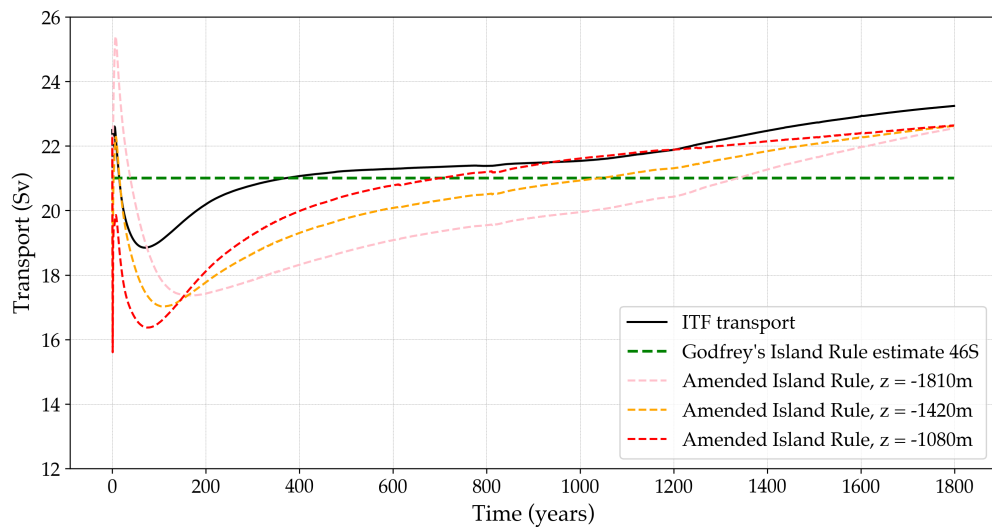
(b) Results for Path 46S

Figure 4.7: Time series of the ITF transport for the simulation with normal wind forcing (WIND1). In black, the ITF transport computed with stream function Ψ is displayed. In blue (a) and green (b), the estimates by Godfrey's Island Rule are displayed for Path 42S and Path 46S respectively. In pink, orange and red the transport estimated by the amended Island Rule at upwelling depths of 1810 m, 1420 m and 1080 m respectively is shown.

4.2.1   WIND1: Normal wind

The results for WIND1 are shown in Figure 4.7. The black line represents the actual flow computed by Ψ, just like in Figure 4.5. In pink, orange and red, the transport estimated by the amended Island Rule at different depths of upwelling is shown.

In both Figure 4.7a and 4.7b, we see that the values for the amended Island Rule improve the estimate in respect to Godfrey's Island Rule. The trend that the actual flow is showing is also seen in the results for the amended Island Rule. In Figure 4.7a, for Path 42S, we see that the amended Island Rule calculated at a depth of 1080 meters (the dashed red line), matches the actual transport best in the last 800 years, deviating 1 to 2 Sv. In Figure 4.7b, for Path 46S, the amended Island Rule calculated at the same depth of 1080 meters, matches the actual flow best in the last 800 years, deviating 0 to 1 Sv. In this case, the results for the amended Island Rule calculated at depths of 1420 and 1810 meters seem to improve in time. After 1800 years, the estimate of the amended Island Rule seems to give the same result for all three depths for Path 46S.

4.2.2   WIND2: Doubled wind

The results for WIND2 are shown in Figure 4.8. Note that for both paths, the amended Island Rule improves the estimate relative to Godfrey's Island Rule. In Figure 4.8a, the results for Path 42S are displayed. We see that the amended Island Rule calculated at a depth of 1080 meters gives the best estimate in the last 800 years with a deviation of 1 to 1, 5 Sv. We also notice that the moment of reaching equilibrium is estimated quite good for all three depths. The results for Path 46S are displayed in Figure 4.8b. We see that the amended Island Rule calculated at a depth of 1420 meters estimates the actual flow best.
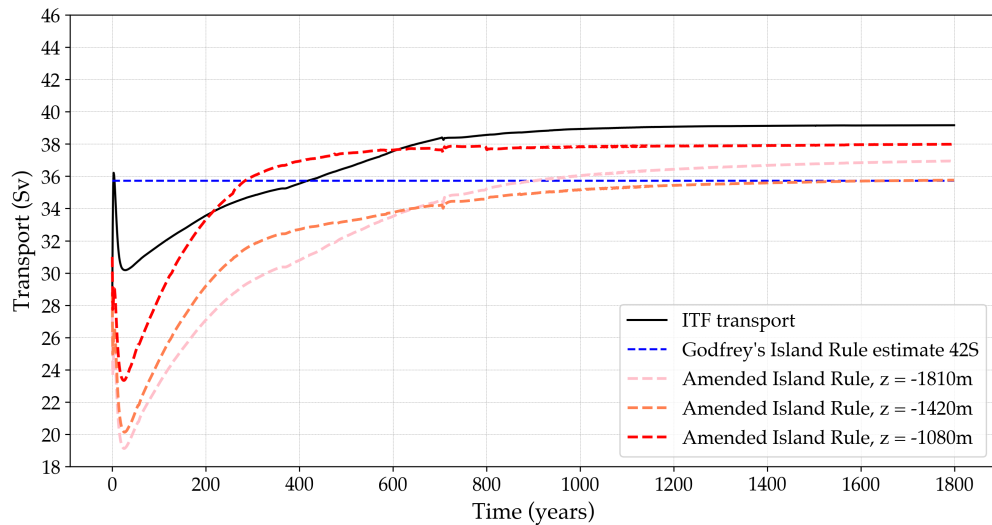
(a) Results for Path 42S
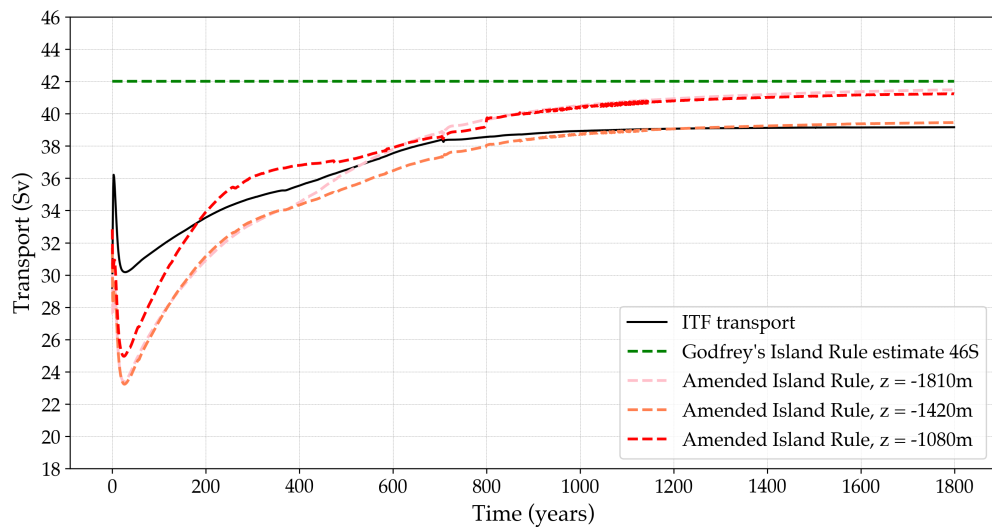
(b) Results for Path 46S

Figure 4.8: Time series of the ITF transport for the simulation with normal wind forcing (WIND2). In black, the ITF transport computed with stream function Ψ is displayed. In blue (a) and green (b), the estimates by Godfrey's Island Rule are displayed for Path 42S and Path 46S respectively. In pink, orange and red the transport estimated by the amended Island Rule at upwelling depths of 1810 m, 1420 m and 1080 m respectively is shown.

4.3   Comparison of the Island Rules

In this section we will compare all Island Rules to see which one estimates the actual flow best. We do this for both simulations.
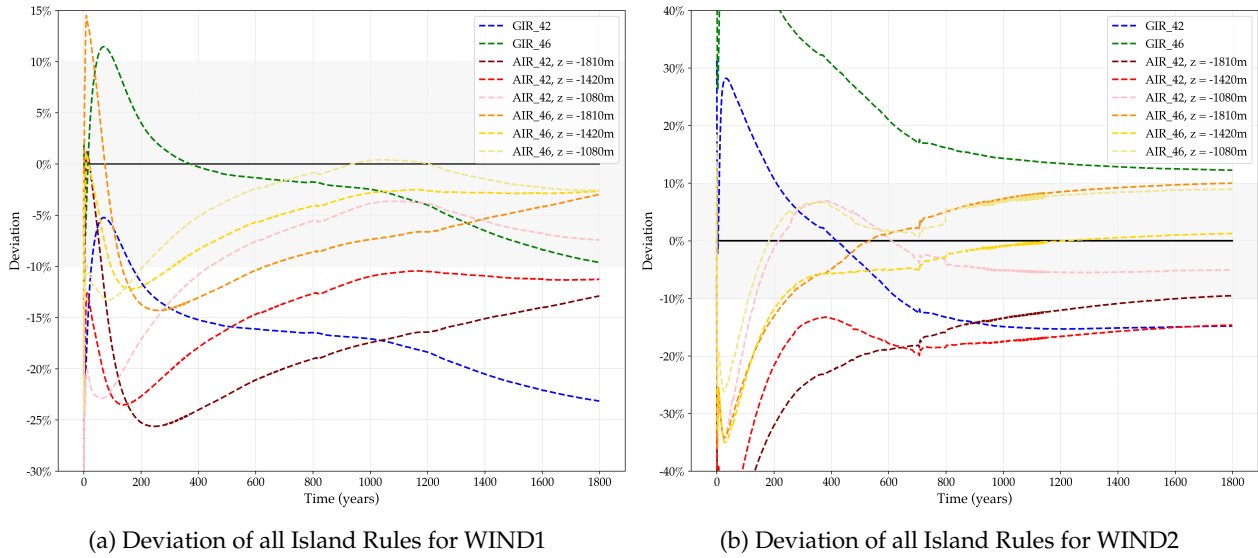

(a) Deviation of all Island Rules for WIND1

(b) Deviation of all Island Rules for WIND2

Figure 4.9: Time series of the deviation in percentages for all calculated Island Rules (Godfrey's Island Rule (GIR) and amended Island Rule (AIR)) in respect to the actual flow for simulation WIND1 (a) and simulation WIND2 (b). Dashed lines represent deviation for the various Island Rules. The grey area runs from -10% to 10%, denoting the acceptable deviation.

In Figure 4.9, the time series of the deviation for all Island Rules is displayed. The grey area runs from -10% to 10%, representing the deviation that we find acceptable. It is most interesting to look at the last 800 years, since during these years the deep ocean has more or less reached equilibrium (Figure 4.4). For WIND1 (Figure 4.9a), we see that the best estimates are given by the amended Island Rule calculated at Path 46S, especially the one calculated at depth $[z = -1080\,\mathrm{m}]$. For WIND2 (Figure 4.9b), we notice that the best estimates are given by the amended Island Rule calculated at Path 46S as well. The very best result is given by the integration depth $[z = -1420\,\mathrm{m}]$.

All code and scripts that are used to obtain our results, can be found here:
https://github.com/FrankaJes/research_ITF_veros_2020.git.

5 Discussion

5.1 Calculation of the actual flow

As explained in Section 3.2, there was some trouble with stream function Ψ in the model output. The stream function was not written to the output files for cells which lay outside the velocity grids. This is solved now in a new setup, but, unfortunately, there was not enough time to rerun all simulations. For now, we have calculated the actual flow using the cell at $[x = 128, y = -8]$, denoted by the yellow cross in Figure 4.2. In Appendix A.1 more is explained about the error that is made here. It is estimated to be $+0,16$ Sv for WIND1 and $+0,24$ Sv for WIND2. This error does not influence our final results significantly, though it can be avoided in future research.

5.2 Assumption of geostrophy

Godfrey's Island Rule is based on the geostrophic balance. However, the segment CD of Figure 3.4 lies very close to the equator, where the geostrophic balance does not hold, due to the absence of the Coriolis force here [6]. This makes us wonder if the assumption of geostrophic balance in the Island Rule is valid for the region we are looking at. Initially, we would not expect this to be a problem since Godfrey designed his Island Rule for this particular area. One might say that normally the CD contribution to the flow is relatively small compared to that of the AB segment. However, in our model, segment CD contributes about 20% to the total estimate. In a geostrophic flow, water moves along the lines of equal pressure, which are called isobars [19]. For the southern hemisphere, when viewing in the direction of the flow, high pressure is to the left and low pressure is to the right. To check if the geostrophic balance holds in our model at latitude 2S (where segment AB is located), we could check if the flow indeed follows the isobars in that area.

5.3 Assumption of steady flow

Another assumption that is made in Godfrey's Island Rule, is that the flow must have reached a steady state. If this is the case, the first term on the right-hand side of Equation (6) vanishes. In our results for WIND1 (Figure 4.5a), we note that the transport of the ITF is still increasing in time. Furthermore, we notice that the the deep ocean is not yet in equilibrium in Figure 4.4a. This would be a reason to believe that the assumption of steady flow does not hold in this case. For WIND2 however, the deep ocean seems to be in equilibrium (Figure 4.4b) and also the ITF transport seems to be stable after 1000 years (Figure 4.5b). An explanation for the flow being more steady for WIND2, could be that this simulation started from a restart file from WIND1 after 1000 years. Because of that, the ocean was already in motion at the start of WIND2, which could explain why the flow in WIND2 reaches an equilibrium earlier than the flow in WIND1.

5.4 Calculation of the Pacific upwelling

The Pacific upwelling is added to Godfrey's Island Rule to obtain our results for the amended Island Rule. We have calculated the upwelling by integrating the vertical transport at three different depths $[z = -1810\,\text{m}, z = -1420\,\text{m}, z = -1080\,\text{m}]$. Note that the actual thermocline varies in depth and it would be more precise to calculate it using that exact depth for every grid cell. However, this is complicated in a configuration like we used, which only has 15 vertical levels. The reason to choose the depths mentioned above is because this defines the boundary between the deep ocean and the wind-driven circulation best. This can also be observed in Figure 4.3, where the MOC is displayed after 1800 years. Furthermore, the upwelling could be calculated using a different approach. One could obtain it by calculating the meridional overturning stream function for just the Pacific Ocean by zonally integrating the meridional velocity, v, for each depth layer. Using this solution, the vertical transport is obtained by taking the meridional integral from 42S or 46S to 80S. These results might differ slightly from our results for the upwelling.

5.5 Resolution of the model

In their paper, Feng *et al.* [10] use a near-global $1/10°$ ocean general circulation model to verify the amended Island Rule. The resolution of our model ($4°$) is very low compared to theirs. To improve our results, we

could run the same simulations on a higher resolution configuration, for example the one-degree model of Veros. This would be an improvement, also considering that the one-degree configuration of Veros includes 115 vertical levels. For example, the bathymetry would be more realistic and the island structure of the Indonesian Archipelago would be more pronounced. Furthermore, we could integrate the wind following a more exact path along the coast, since there is more wind data available. Because of the 115 vertical levels, the calculation of the Pacific upwelling for the amended Island Rule could also be improved, since we expect a better representation of the MOC. However, the resolution of this model is still not high enough to run eddy-rich simulations. Unfortunately, the one-degree model can not be run on a personal laptop due to the computing power that is needed.

6   Summary and Conclusions

In this thesis, our goal was to check to what extent the estimate of Godfrey's Island Rule agrees with the actual Indonesian Throughflow using simulations. Additionally, we looked at the amended Island Rule proposed by Feng *et al.* in 2017 and studied if this would improve the estimate. The derivation of Godfrey's Island Rule and the motivation for the amended Island Rule were discussed in Section 2. Godfrey's Island Rule is based on the geostrophic balance and the Sverdrup balance. Furthermore, it is assumed that dissipation can be ignored, non-linearity is negligible, and the flow has reached a steady state. The model we used to run our simulations is Veros, the Versatile Ocean Simulator. We used the four-degree configuration, which has 15 vertical levels. Two different simulations were run for 1800 model years. The first simulation (WIND1) was forced by normal wind and the second simulation (WIND2) was forced by doubled wind.

We found that Godfrey's Island Rule estimates a flow of the right order of magnitude for both simulations. Two paths of the wind were studied, one with segment AB (Figure 3.4) at 42S (Path 42S) and one at 46S (Path 46S). For Godfrey's Island Rule, we find that in our first simulation, forced by normal wind, the estimate of Path 46S agrees best with the actual flow. What we do notice is that the flow does not reach a steady state. This could be explained by the fact that the deep ocean is not in equilibrium yet, as is seen in Figure 4.4a. In the second simulation, forced by double wind, we see that both estimates of Godfrey's Island Rule predict a strength that deviates $\pm 3\,\mathrm{Sv}$ from the actual flow. Path 42S estimates a weaker flow, whereas Path 46S estimates a stronger flow.

For the amended Island Rule, we calculated the upwelling (Figure 4.6) by integrating the vertical transport at three different depths $[z = -1810\,\mathrm{m}, z = -1420\,\mathrm{m}, z = -1080\,\mathrm{m}]$. This upwelling was added to Godfrey's Island Rule and our results show that this improves the estimate for the actual flow. For WIND1, the amended Island Rule at Path 46S and depth $[z = -1080\,\mathrm{m}]$ estimates the actual flow best. For WIND2, we found that the amended Island Rule at Path 46S and depth $[z = -1420\,\mathrm{m}]$ estimates the actual flow best. This is also seen in Figure 4.9, where the deviation for all Island Rules and for both simulations are displayed in percentages.

Some discussion points are discussed in Section 5. The calculation of the actual flow was not exact. The exact flow is about $0,16\,\mathrm{Sv}$ stronger for WIND1, and $0,24\,\mathrm{Sv}$ stronger for WIND2. In the updated model, this problem does not occur anymore. Furthermore, we saw that the flow for WIND1 had not reached equilibrium after 1800 years. While in Godfrey's Island Rule, it is assumed that the flow is in a steady state. Additionally, both Island Rules are based on the geostrophic balance. Since segment CD (Figure 3.4) lies very close to the equator, one might question if the geostrophic balance holds here. Other discussion points were the calculation of the pacific upwelling and the relatively low resolution of the model. To improve the calculation of the upwelling, it would be good to consider a higher resolution model. Furthermore, higher resolution models, incorporating the island structure of the Indonesian Archipelago, would give a more realistic view of the region. Therefore, higher resolution models would be more applicable to reality.

Our results suggest that the amended Island Rule is an improvement on Godfrey's Island Rule in this particular problem with the ITF. This implies that pacific upwelling influences the strength of the ITF. In future

climate, a weakening trend of upwelling in the Pacific is predicted, due to enhanced greenhouse gas forcing [24]. The slowdown of the upwelling may affect the strength of the ITF as well, which has an impact on global ocean circulation.

7   Outlook

This study showed that the amended Island Rule improves the estimate of Godfrey's Island Rule, implying that Pacific upwelling influences the strength of the ITF. For now, we only used two different (yearly constant) wind forcings. To study to what extent, and how quickly the ITF responds to wind forcing, one could look at yearly varying forcing.

Moreover, it would be useful to study this in an ocean model with higher resolution. That way, the island structure of the Indonesian Archipelago would be more pronounced. Furthermore, in a higher resolution model, we would expect a better representation of the MOC, which would lead to a more exact calculation of the Pacific upwelling. Also, eddy-rich models should be considered to give better insights on reality.

Additionally, it would be interesting to study both Island Rules in coupled atmosphere, ocean, ice, and land models. For example, ENSO could be studied in these coupled models. Also, global warming and greenhouse gas forcing could be simulated in these models. In some simulations of future climate, a weakening of the MOC is predicted [24]. It would be interesting to see if the amended Island Rule would work in these models.

Lastly, it would be interesting to look at other islands in the ocean basin. For example, the flow around New-Zealand or Madagascar could be studied. At these latitudes the geostrophic balance is not questionable, thus making it interesting to see if the Island Rule estimates the flow better.

Acknowledgements

References

[1] *Circulation of the seas — national geographic society.* `https://www.nationalgeographic.org/activity/circulation-seas/`. (Accessed on 05/29/2020).

[2] *A short introduction to veros — veros 0.2.2+2.ge01db96.dirty documentation.* `https://veros.readthedocs.io/en/latest/quickstart/introduction.html`. (Accessed on 05/26/2020).

[3] *To/pyom2/4x4 global model - ifm wiki.* `https://wiki.cen.uni-hamburg.de/ifm/TO/pyOM2/4x4%20global%20model#Forcing_files`. (Accessed on 05/29/2020).

[4] W. CAI, T. COWAN, S. GODFREY, AND S. WIJFFELS, *Simulations of processes associated with the fast warming rate of the southern midlatitude ocean*, Journal of Climate, 23 (2010), pp. 197–206.

[5] W. CAI, G. SHI, T. COWAN, D. BI, AND J. RIBBE, *The response of the southern annular mode, the east australian current, and the southern mid-latitude ocean circulation to global warming*, Geophysical Research Letters, 32 (2005).

[6] B. CUSHMAN-ROISIN AND J.-M. BECKERS, *Introduction to geophysical fluid dynamics: physical and numerical aspects*, Academic press, 2011.

[7] J. DU, B. A. HALEY, A. C. MIX, M. H. WALCZAK, AND S. K. PRAETORIUS, *Flushing of the deep pacific ocean and the deglacial rise of atmospheric co 2 concentrations*, Nature Geoscience, 11 (2018), pp. 749–755.

[8] C. EDEN, *pyOM2.0 documentation*, Institut für Meereskunde, Universität Hamburg, Germany, Aug. 2014.

[9] M. FENG, N. ZHANG, L. QINYAN, AND S. WIJFFELS, *The indonesian throughflow, its variability and centennial change*, Geoscience Letters, 5 (2018).

[10] M. FENG, X. ZHANG, B. SLOYAN, AND M. CHAMBERLAIN, *Contribution of the deep ocean to the centennial changes of the indonesian throughflow*, Geophysical Research Letters, 44 (2017), pp. 2859–2867.

[11] G. A. GLATZMAIER, *Introduction to modeling convection in planets and stars: Magnetic field, density stratification, rotation*, Princeton University Press, 2013.

[12] J. GODFREY, *A sverdrup model of the depth-integrated flow for the world ocean allowing for island circulations*, Geophysical & Astrophysical Fluid Dynamics, 45 (1989), pp. 89–112.

[13] J. GODFREY AND T. GOLDING, *The sverdrup relation in the indian ocean, and the effect of pacific-indian ocean throughflow on indian ocean circulation and on the east australian current*, Journal of Physical Oceanography, 11 (1981), pp. 771–779.

[14] A. GORDON, *Oceanography of the indonesian seas and their throughflow*, Oceanography, 18 (2005), pp. 14–27.

[15] A. L. GORDON, *Interocean exchange of thermocline water*, Journal of Geophysical Research: Oceans, 91 (1986), pp. 5037–5046.

[16] D. HÄFNER, R. L. JACOBSEN, C. EDEN, M. R. B. KRISTENSEN, M. JOCHUM, R. NUTERMAN, AND B. VINTER, *Veros v0.1 – a fast and versatile ocean simulator in pure python*, Geoscientific Model Development, 11 (2018), pp. 3299–3312.

[17] D. A. HODGSON AND L. C. SIME, *Southern westerlies and co 2*, Nature Geoscience, 3 (2010), pp. 666–667.

[18] Q. LIU, D. WANG, W. ZHOU, Q. XIE, AND Y. ZHANG, *Covariation of the indonesian throughflow and south china sea throughflow associated with the 1976/77 regime shift*, Advances in Atmospheric Sciences, 27 (2010), p. 87.

[19] J. MARSHALL AND R. A. PLUMB, *Atmosphere, ocean and climate dynamics: an introductory text*, Academic Press, 1989.

[20] J. P. MCCREARY, S. R. SHETYE, AND P. K. KUNDU, *Thermohaline forcing of eastern boundary currents: With application to the circulation off the west coast of australia*, Journal of Marine Research, 44 (1986), pp. 71–92.

[21] G. MEYERS, *Variation of indonesian throughflow and the el niño-southern oscillation*, Journal of Geophysical Research: Oceans, 101 (1996), pp. 12255–12263.

[22] D. NOF, *The "separation formula" and its application to the pacific ocean*, Deep Sea Research Part I: Oceanographic Research Papers, 45 (1998), pp. 2011–2033.

[23] J. PEDLOSKY, L. J. PRATT, M. A. SPALL, AND K. R. HELFRICH, *Circulation around islands and ridges*, Journal of Marine Research, 55 (1997), pp. 1199–1251.

[24] A. SEN GUPTA, S. MCGREGOR, E. VAN SEBILLE, A. GANACHAUD, J. N. BROWN, AND A. SANTOSO, *Future changes to the indonesian throughflow and pacific circulation: The differing role of wind and deep circulation changes*, Geophysical Research Letters, 43 (2016), pp. 1669–1678.

[25] J. SPRINTALL, S. WIJFFELS, A. L. GORDON, A. FFIELD, R. MOLCARD, R. D. SUSANTO, I. SOESILO, J. SOPAHELUWAKAN, Y. SURACHMAN, AND H. M. VAN AKEN, *Instant: A new international array to measure the indonesian throughflow*, Eos, Transactions American Geophysical Union, 85 (2004), pp. 369–376.

[26] J. SPRINTALL, S. E. WIJFFELS, R. MOLCARD, AND I. JAYA, *Direct estimates of the indonesian throughflow entering the indian ocean: 2004–2006*, Journal of Geophysical Research: Oceans, 114 (2009).

[27] G. A. VECCHI, B. J. SODEN, A. T. WITTENBERG, I. M. HELD, A. LEETMAA, AND M. J. HARRISON, *Weakening of tropical pacific atmospheric circulation due to anthropogenic forcing*, Nature, 441 (2006), pp. 73–76.

[28] R. C. WAJSOWICZ, *The circulation of the depth-integrated flow around an island with application to the indonesian throughflow*, Journal of Physical Oceanography, 23 (1993), pp. 1470–1484.

[29] K. WYRTKI, *Physical oceanography of the Southeast Asian waters*, vol. 2, University of California, Scripps Institution of Oceanography, 1961.

[30] W. ZHUANG, M. FENG, Y. DU, A. SCHILLER, AND D. WANG, *Low-frequency sea level variability in the southern indian ocean and its impacts on the oceanic meridional transports*, Journal of Geophysical Research: Oceans, 118 (2013), pp. 1302–1315.

A Appendix

A.1 Stream function

To calculate the actual flow we needed the stream function Ψ at the coast of Australia. Unfortunately in our simulations, Ψ was not written for those coast grid cells. In the updated model, this is now solved. Since we did not have enough time to rerun all our simulations, we chose to calculate the flow using the stream function value at $[x = 128, y = -8]$. This grid cell is indicated by a yellow cross in Figure 4.2. To check the difference between the exact flow (calculated at the coast of Australia) and the flow calculated using grid cell $[x = 128, y = -8]$, we ran the last 400 years of both simulation using the updated model. In Figure A.1, the difference between Ψ calculated at the coast of Australia (i.e. $[x = 128, y = -12]$), and Ψ calculated at $[x = 128, y = -8]$ is shown for the last 400 years of our simulations. For WIND1, we see that the actual flow is about $+0,16$ Sv stronger than our estimate calculated at $[x = 128, y = -8]$. For WIND2, the actual flow is about $+0,24$ Sv stronger than our estimate. Other grid cells were considered as well, but this one estimated the flow best.
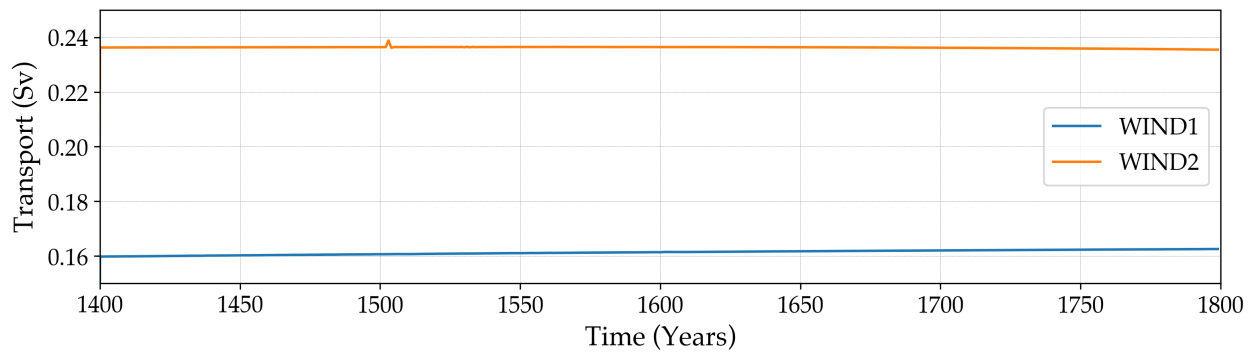

Figure A.1: Difference between Ψ calculated at the coast of Australia (i.e. $[x = 128, y = -12]$), and Ψ calculated at $[x = 128, y = -8]$ in Sverdrups (Sv).